



Probing the structure, stability and hydrogen storage properties of calcium dodecahydro-*closo*-dodecaborate

Vitalie Stavila^{a,*}, Jae-Hyuk Her^{c,d}, Wei Zhou^{c,d}, Son-Jong Hwang^e, Chul Kim^{e,1}, Leigh Anna M. Ottley^b, Terrence J. Udovic^c

^a Sandia National Laboratories, Livermore, CA 94551, United States

^b Sandia National Laboratories, Albuquerque, NM 87106, United States

^c NIST Center for Neutron Research, National Institute of Standards and Technology, Gaithersburg, MD 20899, United States

^d Department of Materials Science and Engineering, University of Maryland, College Park, MD 20742, United States

^e Division of Chemistry and Chemical Engineering, California Institute of Technology, Pasadena, CA 91125, United States

ARTICLE INFO

Article history:

Received 27 October 2009

Received in revised form

16 March 2010

Accepted 16 March 2010

Available online 20 March 2010

Keywords:

Calcium dodecahydro-*closo*-dodecaborate

Hydrogen storage

Metal borohydrides

X-ray and neutron techniques

Density functional theory

ABSTRACT

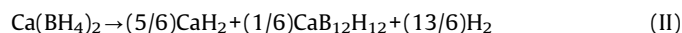
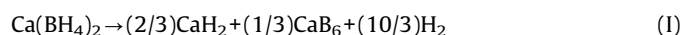
Calcium borohydride can reversibly store up to 9.6 wt% hydrogen; however, the material displays poor cyclability, generally associated with the formation of stable intermediate species. In an effort to understand the role of such intermediates on the hydrogen storage properties of $\text{Ca}(\text{BH}_4)_2$, calcium dodecahydro-*closo*-dodecaborate was isolated and characterized by diffraction and spectroscopic techniques. The crystal structure of $\text{CaB}_{12}\text{H}_{12}$ was determined from powder XRD data and confirmed by DFT and neutron vibrational spectroscopy studies. Attempts to dehydrogenate/hydrogenate mixtures of $\text{CaB}_{12}\text{H}_{12}$ and CaH_2 were made under conditions known to favor partial reversibility in calcium borohydride. However, up to 670 K no notable formation of $\text{Ca}(\text{BH}_4)_2$ (during hydrogenation) or CaB_6 (during dehydrogenation) occurred. It was demonstrated that the stability of $\text{CaB}_{12}\text{H}_{12}$ can be significantly altered using CaH_2 as a destabilizing agent to favor the hydrogen release.

Published by Elsevier Inc.

1. Introduction

Metal borohydrides have attracted increasing interest as promising materials with significant potential for hydrogen storage applications [1–4]. However, there are a number of factors that limit their utility, including high dehydrogenation temperatures and slow kinetics. Vajo et al. [5] proposed a destabilization approach to modify the thermodynamic properties of LiBH_4 using MgH_2 . A number of other additives including CaH_2 , ScH_2 , TiH_2 , and various metals were found to display similar destabilizing effects [6,7]. While there has been some progress in decreasing the dehydrogenation temperatures of borohydrides by destabilization, the problem of poor cycling characteristics remains largely unsolved. There have been reports indicating that $[\text{B}_{12}\text{H}_{12}]^{2-}$ species are formed as intermediates during the thermal decomposition of metal borohydrides [8–11].

Recently Ozolins et al. [12] used theoretical first-principle methods to predict the enthalpies for the following two decomposition pathways for $\text{Ca}(\text{BH}_4)_2$:



The two reactions turn out to have almost identical enthalpies, $\approx 40 \text{ kJ/mol H}_2$. A slightly lower value of 32 kJ/mol H_2 for the enthalpy of reaction (I) was reported from calculations by Miwa et al. [13]. While the thermodynamic characteristics of the two reactions seem to be similar, the amounts of hydrogen released differ significantly in (I) and (II) and correspond to 9.6% and 6.3% mass fraction of hydrogen. Using the prototype electrostatic ground state (PEGS) method, the authors predicted the crystal structures of $\text{CaB}_{12}\text{H}_{12}$, $\text{MgB}_{12}\text{H}_{12}$, and $\text{Li}_2\text{B}_{12}\text{H}_{12}$ [12]. The crystal structures are critical for the evaluation of the thermodynamic characteristics of the reactions involving these species [12,14]. Unfortunately, no experimental data were available in the literature concerning the Ca and Mg salts to confirm the predicted structures.

The reverse reaction of (I) has been shown to occur in moderate yield at 713 K and 70 MPa when CaH_2 and CaB_6 reacted

* Corresponding author at: Sandia National Laboratories, Livermore, CA 94551, United States. Fax: +925 294 3231.

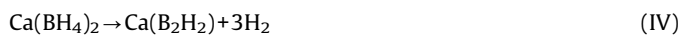
E-mail address: vnstavi@sandia.gov (V. Stavila).

¹ Current address: Department of Chemistry, Hannam University, Daejeon, South Korea.

in the presence of TiCl_3/Pd [15]. Aoki et al. [16] reported that the plateau pressure for $\text{Ca}(\text{BH}_4)_2$ at 593 K is around 0.6 MPa and the amount of H_2 desorbed is 5.9 wt%. It has to be noted that the amount of H_2 released in reaction (II) can be achieved at ≈ 653 K in pure $\text{Ca}(\text{BH}_4)_2$ [17] and at slightly lower temperatures when various additives are used [18]. At higher temperatures, Kim et al. [19] found that about 8.3% mass fraction of H_2 is released in the presence of NbF_5 and suggested that CaB_6 and NbB_2 might be among the decomposition products. Based on *in situ* XRD analysis, the hydrogen release reaction was described as follows [17]:



Recently, Riktor et al. [20] reported that upon heating $\text{Ca}(\text{BH}_4)_2$ to 643–673 K under dynamic vacuum an intermediate phase CaB_2H_x (x most probably equals 2) can be isolated. The decomposition process can be represented in this case by a hypothetical reaction as follows:



The authors suggested that the CaB_2H_x intermediate phase can serve as a precursor for $\text{CaB}_{12}\text{H}_{12}$ [20]. Since the $[\text{B}_{12}\text{H}_{12}]^{2-}$ salts are known to display remarkable thermal and chemical stability [21], it remains unclear whether CaH_2 and $\text{CaB}_{12}\text{H}_{12}$ can be converted into $\text{Ca}(\text{BH}_4)_2$ (reverse reaction of (II)). It also remains to be determined whether reverse reactions (III) and/or (IV) are feasible. The formation of a single solid product (reaction (IV)) may be advantageous in order to avoid phase separation between Ca and B species (reactions (I)–(III)). Despite the appearance of several recent reports on the hydrogen storage properties of $\text{Ca}(\text{BH}_4)_2$, the mechanism by which H_2 is released is still uncertain, and some controversy surrounds the actual products formed during the thermal decomposition, which depends on the temperature regime and additives used.

Possible occurrence of polyborane clusters among the decomposition products, as well as the uncertainty about their rehydriding behavior, has garnered great interest in the scientific community. For that reason we have chosen to explore the synthesis of $\text{CaB}_{12}\text{H}_{12}$ (**1**) and study its hydrogen storage properties. Two precursor complexes, $[\text{Ca}(\text{H}_2\text{O})_7][\text{B}_{12}\text{H}_{12}] \cdot \text{H}_2\text{O}$ [**2**] and $[\text{Ca}(\text{H}_2\text{O})_5(\text{MeCN})_2][\text{B}_{12}\text{H}_{12}]$ (**3**), have been employed to produce crystalline **1** upon dehydration/desolvation. A Rietveld refinement showed that the experimental structure of **1** is largely in accord with the PEGS predicted low-energy monoclinic $C2/c$ model [12] with similar unit cell parameters, but a different unique b -axis. Our density functional theory (DFT) calculations confirm the experimentally refined $C2/c$ structure and correlate well with the phonon density of states (DOS) measured via neutron vibrational spectroscopy (NVS). Hydrogen sorption and desorption studies on mixtures of $\text{CaB}_{12}\text{H}_{12}$ and CaH_2 were performed to understand the different rationales for the dehydrogenation/hydrogenation reactions and the role of the intermediates on the cycling characteristics of $\text{Ca}(\text{BH}_4)_2$.

2. Experimental

2.1. Materials, equipment, and characterization details

Preparations and handling of air-sensitive materials were carried out under a dry Ar atmosphere using standard Schlenk and glovebox techniques. All of the chemicals were of reagent grade and were obtained from Sigma-Aldrich or Strem [24]. Compound **2** and anhydrous $\text{MB}_{12}\text{H}_{12}$ ($M = \text{Mg}, \text{Ca}, \text{and Ba}$) and $\text{M}_2\text{B}_{12}\text{H}_{12}$ ($M = \text{Li}, \text{Na}, \text{K}, \text{and Cs}$) salts were prepared by previously

published procedures [22,23,25]. The reported infrared data were recorded on a Varian 800 FT-IR spectrometer using attenuated total reflectance. Elemental analyses were done at Galbraith Laboratories, Inc. TGA and DSC measurements were performed on Mettler Toledo instruments. SEM and energy dispersive X-ray spectroscopy (EDX) experiments were performed on a FEI scanning electron microscope. Solid-state MAS NMR spectra were measured using a Bruker Avance 500 MHz spectrometer with an 11.7 T magnet and employing a boron-free Bruker 4 mm CPMAS probe. Neutron vibrational spectra were measured using the BT-4 filter analyzer neutron spectrometer [26] at the NIST Center for Neutron Research. First-principles calculations were performed within the plane-wave implementation of the generalized gradient approximation to DFT using a Vanderbilt-type ultrasoft potential with Perdew–Burke–Ernzerhof exchange correlation (Quantum-ESPRESSO package [27]).

2.2. Synthesis of $[\text{Ca}(\text{H}_2\text{O})_5(\text{MeCN})_2][\text{B}_{12}\text{H}_{12}]$, **3**

Cesium dodecahydro-closo-dodecaborate, $\text{Cs}_2\text{B}_{12}\text{H}_{12}$ (932 mg, 2.0 mmol) was dissolved upon heating in 60 mL H_2O and the warm solution was passed through an Amberlite IR-120 ion-exchange column in H^+ form. The acidic fraction represents an aqueous solution of $(\text{H}_3\text{O})_2[\text{B}_{12}\text{H}_{12}]$. The solution was reacted with aqueous $\text{Ca}(\text{OH})_2$ at room temperature until pH=7 was reached. Most of the solvent was removed on a rotary evaporator, and then 20 mL acetonitrile was added. In 2 weeks, crystalline compound **3** was formed in $\sim 30\%$ yield. Anal., Found % (Calcd. %) for $\text{C}_4\text{H}_{28}\text{B}_{12}\text{CaN}_2\text{O}_5$: C, 13.25 (13.57); H, 8.20 (7.97); N, 7.64 (7.91). ATR (cm^{-1}): 3590, 3535, 3508, 3355, 3224, 2478, 2302, 2269, 1615, 1407, 1369, 1204, 1069, 928, 713, 669.

2.3. Synthesis of $\text{CaB}_{12}\text{H}_{12}$, **1**

The anhydrous $\text{CaB}_{12}\text{H}_{12}$ salt was obtained by removal of solvent molecules from **2** or **3** upon heating. In a typical experiment, 750 mg of **3** were loaded into a Schlenk tube and heated in vacuum as follows: (i) at 398 K for 1 h, then (ii) at 498 K for 2 h, and finally (iii) at 573 K for 4 h. The isolated yield was $\sim 85\%$ due to some loss of the fine powder upon heating in vacuum. Anal., Found % (Calcd. %) for $\text{CaB}_{12}\text{H}_{12}$: Ca, 21.1 (22.03); B, 70.2 (71.32); H, 6.79 (6.65). ATR (cm^{-1}): 3683, 3522, 2304, 2473, 1607, 1112, 1081, 753, 730.

2.4. Hydrogenation and dehydrogenation experiments

The hydrogenation attempts were made at 670 K and 100 MPa H_2 pressure. $\text{CaB}_{12}\text{H}_{12}$ and CaH_2 were ground together in a mortar, then placed in a 25-mL hardened steel grinding vial containing two tungsten-carbide balls and milled on a SPEX 8000 high-energy mill for 1 h. The powders were pressed into thin pellets and subjected to 100 MPa pressure H_2 at 670 K for 72 h. The temperature programmed desorption (TPD) experiments were performed on a milled 1:1 $\text{CaB}_{12}\text{H}_{12}:\text{CaH}_2$ sample. After mechanical milling, the samples were transferred into a stainless steel sample holder, which was subsequently attached to a Sieverts apparatus. Pressure changes were monitored with calibrated pressure transducers and recorded by a LabView-based software program.

2.5. Powder X-ray diffraction

X-ray diffraction (XRD) data were obtained at room temperature with a Rigaku Ultima III sealed-tube (1.6 kW, $\text{CuK}\alpha$) diffractometer. The TOPAS-Academic program was used to index

the pattern and to solve the structure. Yet the first attempt failed, probably due to the non-optimal quality powder XRD data. The successful initial structure solution was inspired by the theoretically predicted structure model of Ozolins et al. [12]. Comparing unit-cell parameters, we noticed that the unique axis of the monoclinic lattice was incorrectly assigned, since the β angle was very close to 90° . After changing the assumed unique axis, a new search was performed with molecular (rigid-body) $[\text{B}_{12}\text{H}_{12}]^{2-}$ and Ca^{2+} in direct space. The simulated annealing methods successfully converged and subsequent structure refinement was done with the Rietveld method. Due to the intrinsic deficiency of information in the powder data and the insensitivity of X-rays for H atoms, the rigid body constraints were kept in the final refinement step, but B–B and B–H distances were allowed to vary while the icosahedral symmetry was preserved. All displacement parameters were treated isotropically, and all B and H atoms were constrained to have the same values.

2.6. Single-crystal X-ray structure information

Single-crystals of **3** suitable for X-ray crystallography were separated as small needles from concentrated aqueous solutions of **1** in the presence of MeCN. Crystals were mounted onto a glass fiber from a pool of Fluorolube™ and immediately placed in a cold N_2 vapor stream at 173(2)K, on a Bruker AXS diffractometer equipped with a SMART 1000 CCD detector using graphite monochromatized $\text{MoK}\alpha$ radiation. Lattice determination and data collection were carried out using SMART Version 5.054 software. Data reduction was performed using SAINTPLUS Version 6.01 software and corrected for absorption using the SADABS program within the SAINT software package. The structure was solved by direct methods that yielded the heavy atoms, along with a number of the lighter atoms. The hydrogen atoms were fixed in positions of ideal geometry and refined using SHELXS software. The final refinement of each compound included anisotropic thermal parameters for all non-hydrogen atoms.

3. Results and discussion

Aqueous solutions of $\text{CaB}_{12}\text{H}_{12}$ can be prepared easily by reaction of $(\text{H}_3\text{O})_2[\text{B}_{12}\text{H}_{12}]$ with CaCO_3 [22] or $\text{Ca}(\text{OH})_2$ (this work). The corresponding octahydrate **2** previously reported in the literature was isolated from concentrated aqueous solutions [22,23], while in the presence of acetonitrile, compound **3** was isolated. Completely anhydrous **1** was obtained by heating the solvated compounds **2** or **3** in vacuum up to 573 K. The crystallinity of the anhydrous product was found to depend on the heating rate; slower heating generally resulted in a more crystalline material. The most prominent features of the FTIR vibrational spectra of the $[\text{B}_{12}\text{H}_{12}]^{2-}$ groups in **1–3** are the $\nu(\text{B–H})$ peaks in the region $2500\text{--}2470\text{ cm}^{-1}$ (singlets for **2** and **3** and doublets for **1**), $\delta(\text{B–H})$ peaks around 1080 cm^{-1} and $\nu(\text{B–B})$ near $715\text{--}730\text{ cm}^{-1}$ (Fig. S1, Supplementary material). Complex **3** displays two additional weak bands at 2269 and 2302 cm^{-1} , which can be assigned, respectively, to the stretching $\text{C}\equiv\text{N}$ vibration and a combination mode of CH_3 deformation and C–C stretching vibrations in the acetonitrile molecule. These bands are shifted to higher values by 15 and 9 cm^{-1} from the corresponding peaks at 2254 and 2293 cm^{-1} in pure MeCN.

^1H and ^{11}B MAS NMR of **1** as well as ^{11}B solution NMR of the aqueous solutions prepared from **1** contain characteristic features for $[\text{B}_{12}\text{H}_{12}]^{2-}$ anions (Fig. S2). The solution NMR of **1** confirms the presence of the $[\text{B}_{12}\text{H}_{12}]^{2-}$ units with $J_{\text{B–H}} = 125\text{ Hz}$ [28]. The hydration is shown to narrow both ^1H and ^{11}B NMR signals dramatically; the 4.5 ppm peak in the ^1H NMR spectrum

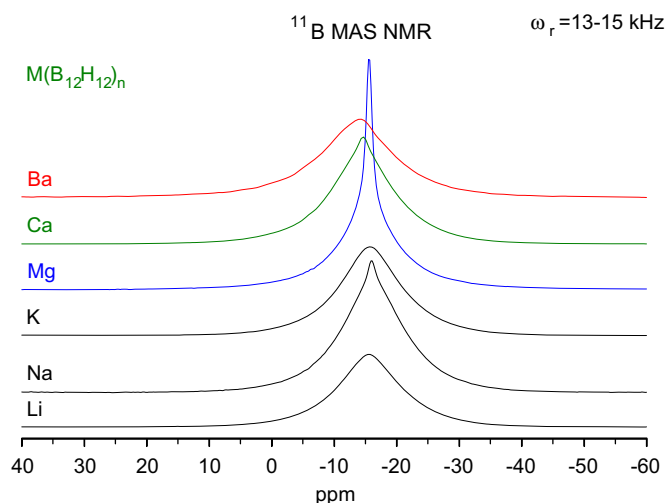


Fig. 1. Center band of ^{11}B MAS NMR spectra of $M_n[\text{B}_{12}\text{H}_{12}]$ ($M = \text{Li, Na, K, Mg, Ca, Ba}$; $n = 1, 2$) salts. The samples were dehydrated by heating under vacuum except the Mg-compound.

corresponds to water protons (Fig. S3). A comparison of the ^{11}B MAS NMR powder spectra for various $M_n\text{B}_{12}\text{H}_{12}$ compounds ($M = \text{Li, K, Na, Mg, Ca, Ba}$; $n = 1, 2$) is shown in Fig. 1. While the center peak position at $\sim 15.5\text{ ppm}$ is similar for all the alkali metals, slight down field shift to $\sim 14.5\text{ ppm}$ is seen for the series of alkaline-earth metals in the current study. The quadrupole coupling of the ^{11}B nucleus also turned out to vary slightly. The fitting of MAS NMR spectra yields quadrupole coupling constants C_Q and η_Q and shift anisotropy parameters (CSA), which reflect the electronic environment around the boron nuclei. The resulting parameters are compiled in Table 1. The calcium salt revealed a smaller quadrupole coupling constant for ^{11}B compared to other cations ($\sim 700\text{ kHz}$) [29], indicating that the icosahedra experience less of field gradient with Ca^{2+} than with alkali metals (see list in Table 1 of Ref. [29]).

Tiritiris and Schleid [22] reported a thermogravimetric analysis of **2**, which showed several dehydration steps with the formation of anhydrous **1** at 497 K . The TGA/DSC analysis of **3** indicates loss of both water and acetonitrile molecules to generate anhydrous **1** at 563 K . The remaining material retains a constant weight between 563 and 693 K . Thereafter, it gradually loses weight, which is attributed to the decomposition of the anhydrous product. The obtained residue at 870 K shows no diffraction in the XRD pattern. The exact nature of the product is not clear, but it shows some residual B–H stretches in the IR spectrum. Solid state NMR characterization of anhydrous **1** after heat treatments at 673 and 723 K under vacuum for 4 h revealed significant changes in ^1H MAS NMR signal intensity ($100\% \rightarrow 93\%$ at 673 K and $100\% \rightarrow 75\%$ at 723 K), which may suggest the loss of one or several hydrogen atoms per icosahedral cage. ^{11}B MAS (Fig. 2a) and ^1H NMR (Fig. 2b) spectra show no significant change in the center band of anhydrous **1** heated at 673 K . Noticeable broadening of the center band peak was observed when the temperature was raised to 723 K . The overall quadrupole powder pattern of heated samples showed a gradual change from the unheated anhydrous **1** to lose the characteristic line shapes of ^{11}B nuclei in the icosahedron, an indication of formation of a disordered state as confirmed by the amorphous nature of the product. While additional investigation is needed to elucidate the structural changes upon heating, we believe that the NMR results may reflect the loss of hydrogen upon heating over 673 K to yield a disordered state as a result of dimer or oligomer formation.

Table 1
NMR parameters of ^{11}B in the $\text{CaB}_{12}\text{H}_{12}$ sample compared to literature data [8,29].

Sample	δ_{iso} (ppm)	δ_{csa} (ppm)	η_{csa}	C_Q (kHz)	η_Q	Lorentzian broadening (Hz)	Gaussian broadening (Hz)
$\text{CaB}_{12}\text{H}_{12}$ (present work)	-14.49 ± 0.03	-133 ± 11	0.2 ± 0.1	600	0.25 ± 0.11	731 ± 238	2230 ± 346
$\text{K}_2\text{B}_{12}\text{H}_{12}$ [8]	-15.0	92	0.15	713	0.2	1200	1204
$\text{K}_2\text{B}_{12}\text{H}_{12}$ [29]	-15.5	-	-	686	-	-	-

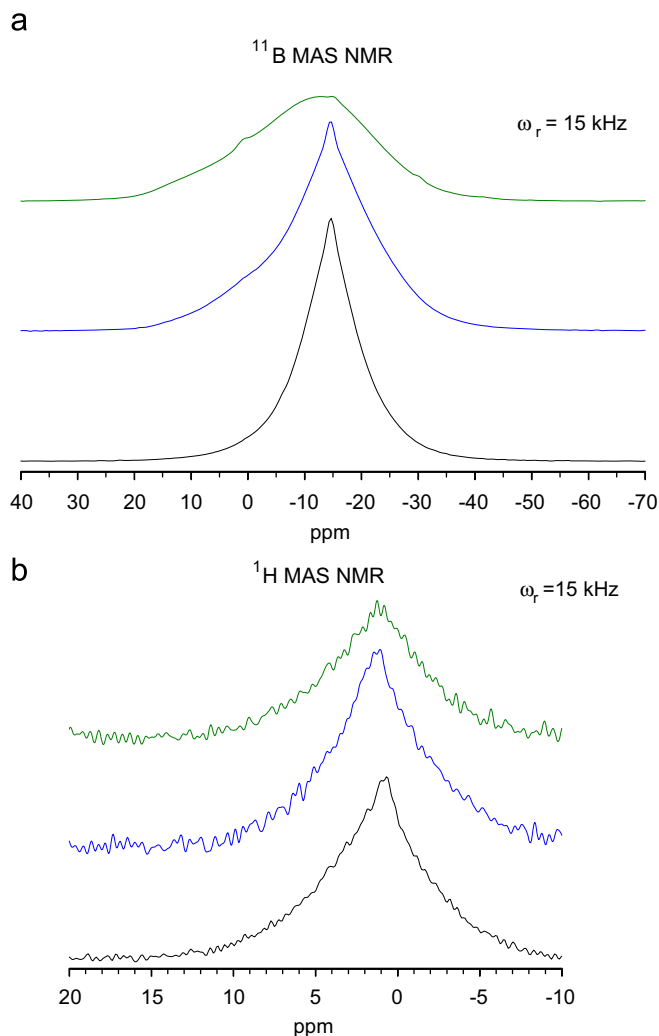


Fig. 2. (a) Center band of ^{11}B MAS NMR spectra for anhydrous **1** (black), heated at 400°C (blue), and heated at 450°C (green). (b) Center band of ^1H MAS NMR spectra for the same samples as in (a). (For interpretation of the references to color in this figure legend, the reader is referred to the web version of this article.)

Anhydrous **1** is soluble in water and can be recrystallized as an octahydrate from aqueous solutions. The products obtained via the dehydration/desolvation of **2** and **3** display identical IR spectra. Powder XRD studies demonstrated that the two products are virtually identical and represent anhydrous **1**. Compound **1** was found to crystallize in a monoclinic unit cell ($C2/c$, $a=7.242(1)\text{\AA}$, $b=11.971(3)\text{\AA}$, $c=10.744(2)\text{\AA}$, $\beta=89.82(3)^\circ$, $V=931.5(3)\text{\AA}^3$, $Z=4$; (see Table 2 and Table S1 in Supplementary material). The structure is similar to the theoretical model predicted by Ozolins et al. [12]; however, the unique b -axis turned out to be different. The crystal structure displays Ca^{2+} cations surrounded by five icosahedral $[\text{B}_{12}\text{H}_{12}]^{2-}$ anions. Three $[\text{B}_{12}\text{H}_{12}]^{2-}$ anions form the triangular

Table 2
Fractional coordinates of **1** (monoclinic, $C2/c$) from powder XRD and DFT relaxation results.

Atoms	x (XRD)	y (XRD)	z (XRD)	x (DFT)	y (DFT)	z (DFT)
Ca	0	0.832(1)	0.25	0	0.8297	0.25
B1	-0.1721	0.2518	0.3242	-0.156	0.234	0.3336
B2	-0.1721	0.0992	0.3242	-0.1586	0.0924	0.3336
B3	0.0677	0.2989	0.3216	0.083	0.2785	0.3107
B4	0.0677	0.0520	0.3216	0.0821	0.0494	0.3118
B5	0.0032	0.1755	0.4116	0.0356	0.1635	0.4022
B6	0.2159	0.1755	0.3199	0.2293	0.1635	0.2978
H1	-0.2966	0.3070	0.3779	-0.2663	0.2848	0.3961
H2	-0.2966	0.0440	0.3779	-0.271	0.0429	0.3937
H3	0.1167	0.3882	0.3733	0.1441	0.3602	0.3537
H4	0.1167	-0.0372	0.3733	0.1464	-0.0305	0.3589
H5	0.0055	0.1755	0.5286	0.0645	0.1634	0.511
H6	0.3721	0.1755	0.3705	0.3933	0.1626	0.3344

The lattice parameters were optimized during the DFT relaxation. The B and H positions were not freely refined. B–B and B–H distances were refined with constrains to 1.826(8) and 1.26(4) \AA , respectively.

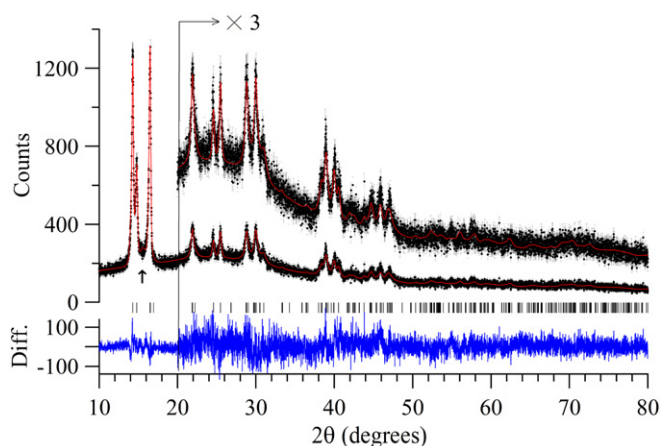


Fig. 3. XRD pattern of anhydrous, polycrystalline $\text{CaB}_{12}\text{H}_{12}$ (**1**) and the Rietveld refinement result. Black: raw data points. Red: calculated profile. Blue: difference curve (observed – calculated) on the same scale. Vertical tick marks: allowed Bragg reflection positions. After $2\theta \approx 20^\circ$, the additional pattern and difference curve are both presented with $3\times$ magnification. The arrow at $\sim 15^\circ$ denotes the position of an additional Lorentzian impurity line attributed to the strongest reflection of the trihydrated phase, $\text{CaB}_{12}\text{H}_{12} \cdot 3\text{H}_2\text{O}$, which was included in the refinement process. (For interpretation of the references to color in this figure legend, the reader is referred to the web version of this article.)

equatorial plane centered on each Ca^{2+} cation, while the other two $[\text{B}_{12}\text{H}_{12}]^{2-}$ anions are located in axial positions. Each Ca^{2+} cation interacts with eight neighboring H atoms from the five $[\text{B}_{12}\text{H}_{12}]^{2-}$ anions. Two H atoms are from each of the three equatorial $[\text{B}_{12}\text{H}_{12}]^{2-}$ anions and one H atom is from each of the two axial $[\text{B}_{12}\text{H}_{12}]^{2-}$ anions. The experimental, fitted, and difference profiles of the XRD patterns are shown in Fig. 3. The structure of **1** and its packing scheme are presented in Figs. 4 and 5. Using DFT, structural

optimizations were performed with respect to atomic positions and lattice parameters. The room-temperature structure from XRD data was numerically relaxed at 0K. The optimized structure was close to that experimentally observed (see Table 2), suggesting that there is no structural phase transition between 0K and room temperature.

The neutron vibrational spectrum for **1** was measured at 4K. Since the total scattering cross section for H is much larger than

that for B or Ca, spectral features are dominated by the various internal vibrational modes of the dodecahydro-*closo*-dodecaborate anions involving hydrogen displacements. For comparison, the phonon density of states (DOS) was calculated from the DFT-optimized structure using the supercell method ($2 \times 2 \times 1$ cell size) with finite displacements [30,31] and was appropriately weighted to take into account the H, B, and Ca total neutron scattering cross sections. The resulting weighted DOS (broadened

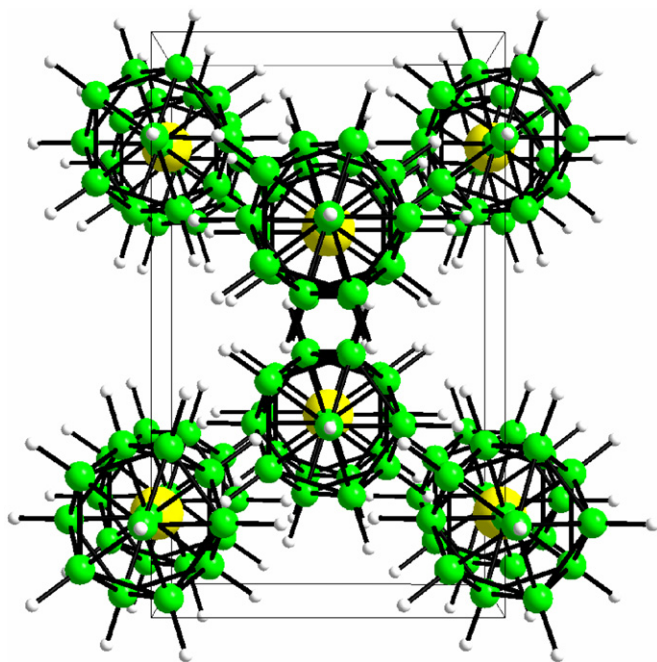


Fig. 4. Crystal structure of **1** in the monoclinic ($C2/c$) unit cell viewed along the c -axis (perspective).

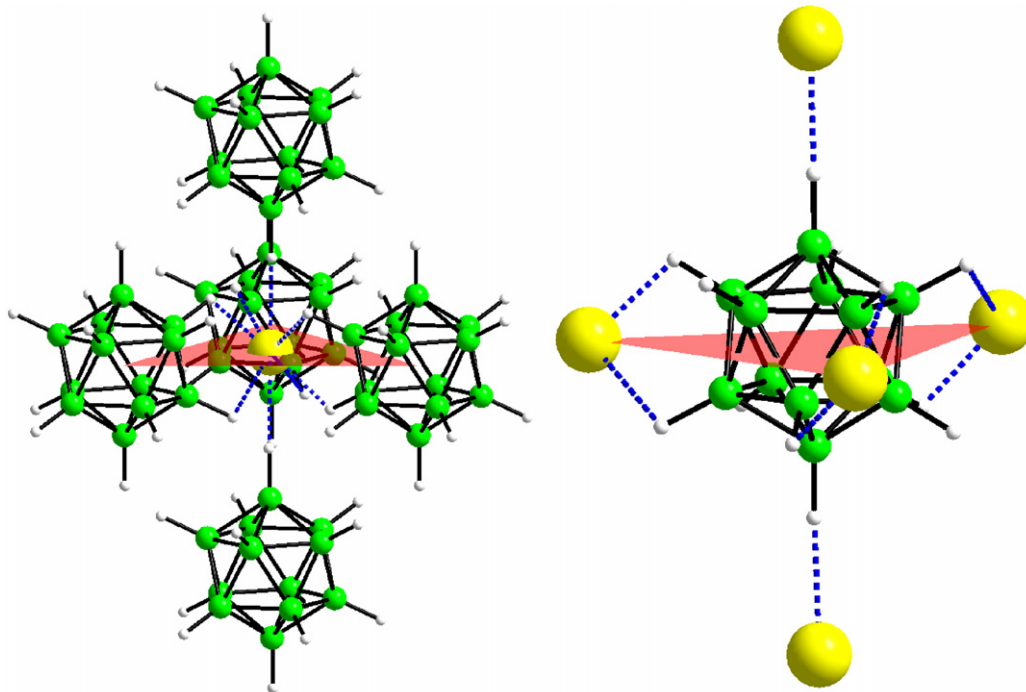


Fig. 5. The packing scheme in **1**. Yellow: Ca, green: B, gray: H, partially transparent red triangle: equatorial plane consisting of three counter anions. Blue dashed lines: Ca...H distances of 2.04(3) Å, 2.22(2) Å, 2.38(4) Å, and 2.46(2) Å. (For interpretation of the references to color in this figure legend, the reader is referred to the web version of this article.)

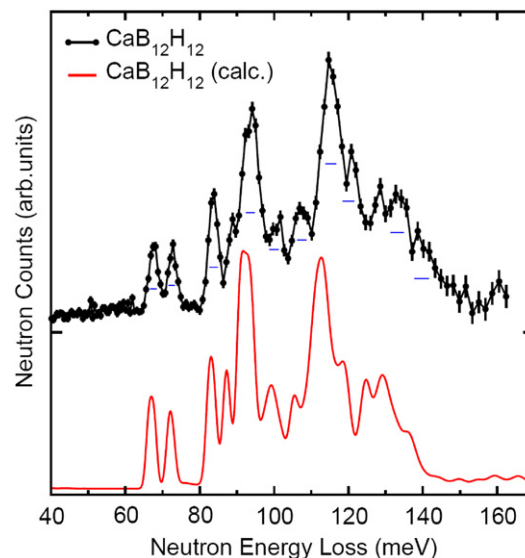


Fig. 6. NV spectrum (black, vertically offset for clarity) of **1** at 4K compared with the calculated (weighted) phonon density of states (red) of the $C2/c$ structure. Horizontal bars represent the full-width-at-half-maximum instrumental resolution and vertical bars show $\pm 1\sigma$ (N.B.: $1 \text{ meV} \approx 8.066 \text{ cm}^{-1}$). (For interpretation of the references to color in this figure legend, the reader is referred to the web version of this article.)

by the known instrumental resolution) is in good agreement with the experimental NVS results (see Fig. 6), providing additional corroboration for the refined $\text{CaB}_{12}\text{H}_{12}$ structure. Previous reports suggest that NVS measurements and phonon DOS calculations are indeed sensitive to the structural details of the $[\text{B}_{12}\text{H}_{12}]^{2-}$ lattice arrangements, as exemplified for $\text{Cs}_2\text{B}_{12}\text{H}_{12}$ [32] and $\text{Li}_2\text{B}_{12}\text{H}_{12}$ [33].

The crystal structures of several anhydrous metal salts of $[\text{B}_{12}\text{H}_{12}]^{2-}$ have been reported to date. $M_2\text{B}_{12}\text{H}_{12}$ salts ($M=\text{K}$, Rb , Cs and Tl) crystallize in a cubic lattice with M^+ cations in the tetrahedral interstices of the ccp-arranged icosahedral $[\text{B}_{12}\text{H}_{12}]^{2-}$ anions. The primitive cubic crystal structure of $\text{Li}_2\text{B}_{12}\text{H}_{12}$ contains Li^+ cations in a strongly distorted octahedral environment formed by six hydrogen atoms of three $[\text{B}_{12}\text{H}_{12}]^{2-}$ groups [33]. The coordination environment of the Na^+ cations in the recently reported monoclinic $P2_1/n$ structure of $\text{Na}_2\text{B}_{12}\text{H}_{12}$ can be viewed as either an octahedron or a cube [34]. Relatively short alkali metal–hydrogen distances are found; for example, $\text{Li}\cdots\text{H}$ distances in $\text{Li}_2\text{B}_{12}\text{H}_{12}$ measure 2.08 and 2.22 Å [33], while the corresponding $M\cdots\text{H}$ distances in $\text{Na}_2\text{B}_{12}\text{H}_{12}$ [34] and $\text{K}_2\text{B}_{12}\text{H}_{12}$ [25] are 2.22–2.86 and 2.94 Å, respectively. The $\text{Ca}\cdots\text{H}$ distances in **1** are 2.04(3), 2.22(2) and 2.46(2) Å for equatorial interactions and 2.38(4) Å for axial interactions. Such distances suggest significant alkali–metal $\cdots\text{H}$ interactions, which seem to be a common feature for anhydrous dodecahydro-*closo*-dodecaborate salts. $[\text{B}_{12}\text{H}_{12}]^{2-}$ is one of the least coordinating anions and in most of the compounds is not part of the first coordination sphere of the metal cation [35,36]. There are very few exceptions, usually involving transition metals in low oxidation state, as in $[(\text{PhMe}_2\text{P})_3\text{RuB}_{12}\text{H}_{12}]$ [37] or $(\text{Bu}_4\text{N})_2\{[1,2\text{-C}_6\text{F}_4\text{Hg}]_3\}_2[\text{B}_{12}\text{H}_{12}]$ [38].

Compound **1** can be stored in a dry atmosphere; in the presence of moisture it tends to absorb water. Thus, about a month later after the initial powder XRD data collection, we revisited the vacuum-grease-sealed capillary specimen of **1** and found that the XRD pattern was completely changed. We attributed this to an imperfect seal allowing a slow uptake of water into the hygroscopic dodecahydro-*closo*-dodecaborate salt. The new powder pattern (Fig. S4) was auto-indexed with a rhombohedral unit cell ($R3c$, $a=11.231(3)$ Å, $c=16.590(4)$ Å in hexagonal setting, $V=1812(1)$ Å³, $Z=6$; see Tables S1 and S2, Supplementary material) and revealed as partially hydrated

$\text{CaB}_{12}\text{H}_{12}$ form, namely trihydrated $\text{CaB}_{12}\text{H}_{12}\cdot 3\text{H}_2\text{O}$. The structure in Fig. 7 displays the Ca^{2+} cation coordinated by three H_2O molecules equatorially and two tridentate $[\text{B}_{12}\text{H}_{12}]^{2-}$ anions occupying the axial positions in the coordination sphere. The cationic $\text{Ca}(\text{H}_2\text{O})_3$ units and anionic $[\text{B}_{12}\text{H}_{12}]^{2-}$ groups form a one-dimensional chain structure along the c -axis of the unit cell. Interestingly enough, in **1**, each Ca^{2+} cation displays bi-tetrahedral surroundings that are reminiscent of the coordination scheme for trihydrated $\text{CaB}_{12}\text{H}_{12}\cdot 3\text{H}_2\text{O}$, in which the three water molecules are replaced by three bi-dentate $[\text{B}_{12}\text{H}_{12}]^{2-}$ anions.

Compound **3** was found to crystallize in the monoclinic space group $P2_1/c$ (see additional structural data in Tables S1, S3, and S4; Supplementary material). The structural parameters of **2** and **3** are quite similar except that in **3**, two water molecules are

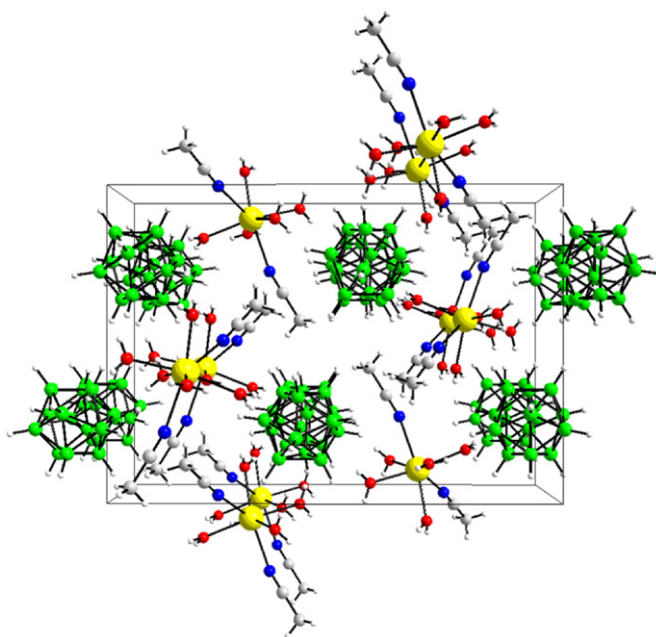


Fig. 8. A view of the crystal structure of **3** along the b -axis.

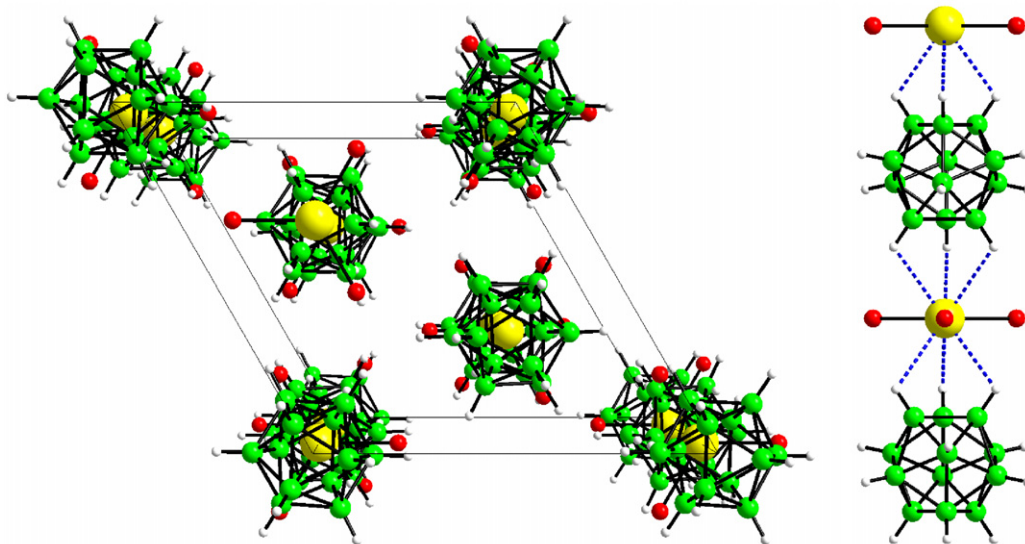


Fig. 7. (Left) $\text{CaB}_{12}\text{H}_{12}\cdot 3\text{H}_2\text{O}$ structure in the hexagonal ($R3c$) unit cell viewed along the c -axis (perspective). (Right) The 1D packing scheme of $\text{CaB}_{12}\text{H}_{12}\cdot 3\text{H}_2\text{O}$. Yellow: Ca^{2+} , green: B, gray: H, red: O^{2-} , blue dashed lines: $\text{Ca}-\text{H}$ bond distances of 2.59(1) Å. The Ca^{2+} cation is surrounded by three equatorial H_2O molecules ($\text{Ca}-\text{O}$: 2.333(7) Å) and two axial tridentate $[\text{B}_{12}\text{H}_{12}]^{2-}$ anions. (For interpretation of the references to color in this figure legend, the reader is referred to the web version of this article.)

substituted with two acetonitrile molecules and the complex has no crystallization water molecules. Fig. 8 shows the unit cell structure of **3**. The compound contains two Ca^{2+} and two $[\text{B}_{12}\text{H}_{12}]^{2-}$ ions in the asymmetric unit. The B–B bond distances and angles in **3** are consistent with the corresponding values reported for the icosahedral clusters in the octahydrate [22]. The 7-fold coordination of the Ca atom (Fig. S5, Supplementary Material) in **3** is defined by five Ca–O bonds with bond distances between 2.339(1) and 2.465(1) Å and two Ca–N bonds, 2.518(1) and 2.550(1) Å. The mean Ca–O distance, 2.399(1) is only slightly shorter than the sum of ionic radii for Ca^{2+} and O^{2-} , 2.44 Å [39].

We are currently investigating the hydrogen absorption properties of $\text{CaB}_{12}\text{H}_{12}$ ball-milled with various metal hydrides. Ball-milling is known to facilitate both hydrogen release and absorption in metal hydrides [40–43]. Our rehydrogenation attempts indicate that the $\text{CaB}_{12}\text{H}_{12}$ sample ball-milled with 5 equiv. of CaH_2 does not form any noticeable amounts of calcium borohydride at 670 K and 100 MPa hydrogen pressure. Interesting enough, when the $\text{CaB}_{12}\text{H}_{12}$:5 CaH_2 mixture is heated in vacuum at 833 K prior to hydrogenation at 100 MPa H_2 pressure and 670 K, small amounts of crystalline $\text{Ca}(\text{BH}_4)_2$ are produced. Although the mechanism by which $\text{Ca}(\text{BH}_4)_2$ is generated requires additional studies, it is possible that CaB_6 is generated *in situ*, and then reacts with CaH_2 to form the borohydride. Based on first-principles calculations, Ozolins et al. [12] predicted that $\text{CaB}_{12}\text{H}_{12}$ can react with 1 equiv. of CaH_2 to generate H_2 (6.3% mass fraction capacity) and CaB_6 :



Our TPD studies on a 1:1 mixture of $\text{CaB}_{12}\text{H}_{12}$ and CaH_2 revealed that at 670 K only 0.8% mass fraction H_2 is released (Fig. S6), in contrast with $\text{Ca}(\text{BH}_4)_2$, which, under these conditions, releases 8.1% mass fraction of hydrogen. An *ex situ* XRD analysis of the product showed no CaB_6 formation up to 670 K. We applied TGA to study the thermal behavior of the materials up to 870 K. Heating the ball-milled $\text{CaB}_{12}\text{H}_{12}$: CaH_2 sample up to 870 K resulted in ~6% mass loss. The weight loss is in good agreement with the calculated amount of H_2 released in reaction (V). Under the same conditions, the mass loss from pure $\text{CaB}_{12}\text{H}_{12}$ is less than 1.5% (Fig. 9). The XRD of the sample resulting from dehydrogenating the 1:1 $\text{CaB}_{12}\text{H}_{12}$: CaH_2 composite confirmed that CaB_6 was formed as a crystalline product of the reaction (Fig. 10). SEM revealed that the resulting material consists of submicron particles interconnected into larger agglomerates (inset in Fig. 10). In contrast, $\text{CaB}_{12}\text{H}_{12}$ thermally treated at 870 K displays an amorphous XRD pattern with no

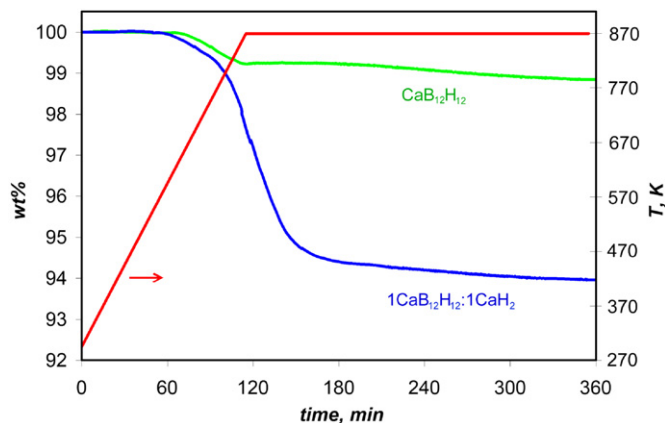


Fig. 9. TGA data for $\text{CaB}_{12}\text{H}_{12}$ and ball-milled $\text{CaB}_{12}\text{H}_{12}$: CaH_2 (1:1).

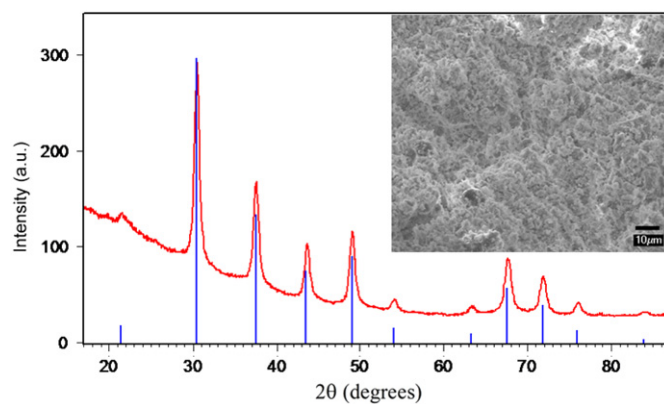


Fig. 10. XRD powder profile of the product generated from ball-milled $\text{CaB}_{12}\text{H}_{12}$: CaH_2 (1:1) upon heating to 870 K and its comparison to the CaB_6 phase, JCPDS No. 00-031-0254. The inset shows the SEM image of the as-obtained powder.

evidence of CaB_6 being formed. The product is hygroscopic as evidenced by the mass increase of the material exposed to moist air. EDX spectroscopy of the sample revealed that in addition to the main Ca and B peaks, the spectrum displays a characteristic oxygen peak. No such peak was detected when $\text{CaB}_{12}\text{H}_{12}$ was decomposed in the presence of CaH_2 to form the air-stable CaB_6 (Fig. S7).

We believe that high kinetic barriers may be responsible for poor hydrogen release and absorption in reactions involving $\text{CaB}_{12}\text{H}_{12}$ up to 670 K. This result is consistent with experimental observation of decreasing hydrogen storage capacity of $M[\text{BH}_4]_m$ systems under similar conditions as desorption/absorption cycles are repeated. Accumulation of $[\text{B}_{12}\text{H}_{12}]^{2-}$ intermediates leads to significant function loss, presumably due to the high stability of the dodecahydro-*closo*-dodecaborate clusters.

4. Conclusions

In the present paper, we demonstrate the synthesis of $\text{CaB}_{12}\text{H}_{12}$ from $[\text{Ca}(\text{H}_2\text{O})_7][\text{B}_{12}\text{H}_{12}] \cdot \text{H}_2\text{O}$ and $[\text{Ca}(\text{H}_2\text{O})_5(-\text{MeCN})_2][\text{B}_{12}\text{H}_{12}]$ and investigate its structure and reactivity. The crystal structure of $\text{CaB}_{12}\text{H}_{12}$ was refined from powder XRD data. NVS data are in agreement with the DFT calculated phonon density of states (DOS) and support the choice of the monoclinic $C2/c$ structure. The rehydrogenation tests on the ball-milled mixtures of $\text{CaB}_{12}\text{H}_{12}$ and CaH_2 did not show any borohydride formation at 100 MPa H_2 pressure and 670 K. Similar to alkali metal dodecahydro-*closo*-dodecaborates, $\text{CaB}_{12}\text{H}_{12}$ displays a remarkable thermal stability. We show that the addition of CaH_2 has a destabilizing effect on $\text{CaB}_{12}\text{H}_{12}$ and favors hydrogen release. The formation of dodecahydro-*closo*-dodecaborate species during the decomposition of $\text{Ca}(\text{BH}_4)_2$ can be disadvantageous with respect to reversible hydrogen storage applications. The accumulation of such stable intermediate species in the reaction mixtures not only decreases the capacity, but also the cyclability of the material. This study highlights a possible mitigation of this problem by using destabilization approaches which modify the reaction pathways and can favor the hydrogen release.

Acknowledgments

The authors would like to acknowledge the many valuable suggestions made by Drs. Ewa Rönnebro, Eric Majzoub, Timothy Boyle and Leonard Klebanoff. We are grateful to

Dr. Satish S. Jalisatgi for generously providing the $\text{Li}_2\text{B}_{12}\text{H}_{12}$ and $\text{K}_2\text{B}_{12}\text{H}_{12}$ samples and to Jeff Chames for help with the SEM/EDX experiments. We gratefully acknowledge financial support from the US Department of Energy, Office of Energy Efficiency and Renewable Energy, in the Hydrogen, Fuel Cells & Infrastructure Technologies Program under Contract nos. DE-AC04-94AL85000, DE-AI-01-05EE11104, and DE-AI-01-05EE11105. The NMR facility at Caltech was supported by the National Science Foundation (NSF) under Grant no. 9724240 and partially supported by the MRSEC Program of the NSF under Award Number DMR-0520565.

Appendix A. Supplementary material

Supplementary data associated with this article can be found in the online version at doi:10.1016/j.jssc.2010.03.026.

References

- [1] A. Züttel, A. Borgschulte, S.I. Orimo, *Scr. Mater.* 56 (2007) 823–828.
- [2] B. Sakintuna, F. Lamari-Darkrim, M. Hirscher, *Int. J. Hydrogen Energy* 32 (2007) 1121–1140.
- [3] Y. Nakamori, H.W. Li, K. Kikuchi, M. Aoki, K. Miwa, S. Towata, S. Orimo, *J. Alloys Compd.* 446 (2007) 296–300.
- [4] S.I. Orimo, Y. Nakamori, J.R. Eliseo, A. Züttel, C.M. Jensen, *Chem. Rev.* 107 (2007) 4111–4132.
- [5] J.J. Vajo, S.L. Skeith, F. Mertens, *J. Phys. Chem. B* 109 (2005) 3719–3722.
- [6] J. Yang, A. Sudik, C. Wolverton, *J. Phys. Chem. C* 111 (2007) 19134–19140.
- [7] J. Purewal, S.J. Hwang, R.C. Bowman, E. Rönnebro, B. Fultz, C. Ahn, *J. Phys. Chem. C* 112 (2008) 8481–8485.
- [8] S.J. Hwang, R.C. Bowman, J.W. Reiter, J. Rijssenbeek, G.L. Soloveichik, J.C. Zhao, H. Kabbour, C.C. Ahn, *J. Phys. Chem. C* 112 (2008) 3164–3169.
- [9] S.I. Orimo, Y. Nakamori, N. Ohba, K. Miwa, M. Aoki, S. Towata, A. Züttel, *Appl. Phys. Lett.* 89 (2006) 021920.
- [10] G.L. Soloveichik, Y. Gao, J. Rijssenbeek, M. Andrus, S. Kniajanski, R.C. Bowman Jr., S.-J. Hwang, J.-C. Zhao, *Int. J. Hydrogen Energy* 34 (2009) 916–928.
- [11] H.W. Li, K. Kikuchi, Y. Nakamori, N. Ohba, K. Miwa, S. Towata, S. Orimo, *Acta Mater.* 56 (2008) 1342–1347.
- [12] V. Ozolins, E.H. Majzoub, C. Wolverton, *J. Am. Chem. Soc.* 131 (2009) 230–237.
- [13] K. Miwa, M. Aoki, T. Noritake, N. Ohba, Y. Nakamori, S. Towata, A. Züttel, S. Orimo, *Phys. Rev. B* 74 (2006) 155122.
- [14] N. Ohba, K. Miwa, M. Aoki, T. Noritake, S. Towata, Y. Nakamori, S. Orimo, A. Züttel, *Phys. Rev. B* 74 (2006) 075110.
- [15] E. Rönnebro, E.H. Majzoub, *J. Phys. Chem. B* 111 (2007) 12045–12047.
- [16] M. Aoki, K. Miwa, T. Noritake, N. Ohba, M. Matsumoto, H.W. Li, Y. Nakamori, S. Towata, S. Orimo, *Appl. Phys. A* 92 (2008) 601–605.
- [17] J.H. Kim, S.A. Jin, J.H. Shim, Y.W. Cho, *J. Alloys Compd.* 461 (2008) L20–L22.
- [18] J.H. Kim, S.A. Jin, J.H. Shim, Y.W. Cho, *Scr. Mater.* 58 (2008) 481–483.
- [19] J.H. Kim, J.H. Shim, Y.W. Cho, *J. Power Sources* 181 (2008) 140–143.
- [20] M.D. Riktor, M.H. Sorby, K. Chlopek, M. Fichtner, B.C. Hauback, *J. Mater. Chem.* 19 (2009) 2754–2759.
- [21] I.B. Sivaev, V.I. Bregadze, S. Sjöberg, *Collect. Czech. Chem. Commun.* 67 (2002) 679–727.
- [22] I. Tiritiris, T. Schleid, *Z. Anorg. Allg. Chem.* 627 (2001) 1836–1845.
- [23] K.A. Solntsev, N.T. Kuznetsov, V.I. Ponomarev, *Inorg. Mater.* 12 (1976) 874–878.
- [24] Certain commercial suppliers are identified in this paper to foster understanding. Such identification does not imply our recommendation or endorsement nor does it imply that the materials or equipment identified are necessarily the best available for the purpose.
- [25] I. Tiritiris, T. Schleid, *Z. Anorg. Allg. Chem.* 629 (2003) 1390–1402.
- [26] T.J. Udovic, D.A. Neumann, J. Leao, C.M. Brown, *Nucl. Instrum. Methods Phys. Res. A* 517 (2004) 189–201.
- [27] <http://www.pwscf.org/>.
- [28] S. Hermanek, *Chem. Rev.* 92 (1992) 325–362.
- [29] I. Tiritiris, T. Schleid, K. Muller, *Appl. Mag. Res.* 32 (2007) 459–481.
- [30] G. Kresse, J. Furthmüller, J. Hafner, *Europhys. Lett.* 32 (1995) 729–734.
- [31] T. Yildirim, *Chem. Phys.* 261 (2000) 205–216.
- [32] D.G. Allis, B.S. Hudson, *J. Phys. Chem. A* 110 (2006) 3744–3749.
- [33] J.-H. Her, M. Yousufuddin, W. Zhou, S.S. Jalisatgi, J.G. Kulleck, J.A. Zan, S.-J. Hwang, R.C. Bowman, T.J. Udovic, *Inorg. Chem.* 47 (2008) 9757–9759.
- [34] J.-H. Her, W. Zhou, V. Stavila, C.M. Brown, T.J. Udovic, *J. Phys. Chem. C* 113 (2009) 11187.
- [35] S.H. Strauss, *Chem. Rev.* 93 (1993) 927–942.
- [36] I.A. Zakharaeva, *Coord. Chem. Rev.* 43 (1982) 313–324.
- [37] M. Elrington, N.N. Greenwood, J.D. Kennedy, M. Thorntonpett, *J. Chem. Soc. Dalton Trans.* (1987) 451–456.
- [38] E.S. Shubina, I.A. Tikhonova, E.V. Bakhmutova, F.M. Dolgushin, M.Yu. Antipin, V.I. Bakhmutov, I.B. Sivaev, L.N. Teplitskaya, I.T. Chizhevsky, I.V. Pisareva, V.I. Bregadze, L.M. Epstein, V.B. Shur, *Chem. Eur. J.* 7 (2001) 3783–3790.
- [39] R.D. Shannon, *Acta Crystallogr. A* 32 (1976) 751–767.
- [40] A. Andreasen, T. Vegge, A.S. Pedersen, *J. Solid State Chem.* 178 (2005) 3672–3678.
- [41] H. Shao, H. Xu, Y. Wang, X. Li, *J. Solid State Chem.* 177 (2004) 3626–3632.
- [42] R.J. Newhouse, V. Stavila, S.-J. Hwang, L.E. Klebanoff, J.Z. Zhang, *J. Phys. Chem. C* 114 (2010) 5224–5232, doi:10.1021/jp9116744.
- [43] H. Li, K. Kikuchi, Y. Nakamori, K. Miwa, S. Towata, S. Orimo, *Scr. Mater.* 57 (2007) 679–682.